THE PURE ROTATIONAL SPECTRA OF DIATOMICS AND HALOGEN-ADDITION BENZENE MEASURED BY MICROWAVE AND RADIO FREQUENCY SPECTROMETERS

Kerry C. Etchison, B.A.

Thesis Prepared for the Degree of

MASTER OF SCIENCE

UNIVERSITY OF NORTH TEXAS

August 2010

APPROVED:

Stephen A. Cooke, Major Professor
Diana S. Mason, Committee Member
William Acree, Chair of the Department of Chemistry
James D. Meernik, Acting Dean of the Robert B. Toulouse School of Graduate Studies

Etchison, Kerry C. *The pure rotational spectra of diatomics and halogen-addition benzene measured by microwave and radio frequency spectrometers*. Master of Science (Chemistry), August 2010, 47 pp., 12 tables, 9 illustrations, references, 63 titles.

Two aluminum spherical mirrors with radii of 203.2 mm and radii of curvature also of 203.2 mm have been used to construct a tunable Fabry–Perót type resonator operational at frequencies as low as 500 MHz. The resonator has been incorporated into a pulsed nozzle, Fourier transform, Balle–Flygare spectrometer. The spectrometer is of use in recording low J transitions of large asymmetric molecules where the spectra are often greatly simplified compared to higher frequency regions. The resonators use is illustrated by recording the rotational spectra of bromobenzene and iodobenzene.

In related experiments, using similar equipment, the pure rotational spectra of four isotopomers of SrS and all three naturally occurring isotopomers of the actinide-containing compound thorium monoxide have been recorded between 6 and 26 GHz. The data have been thoroughly analyzed to produce information pertaining to bond lengths and electronic structures.

Copyright 2010

by

Kerry C. Etchison

ACKNOWLEDGEMENTS

I would like to thank my committee for their time, effort, energy, and support during this process and for providing me the guidance and direction needed to finish my degree.

I am happy to acknowledge numerous conversations with Professor Jens-Uwe Grabow at the University of Hannover. I thank Professor Sean Peebles at Eastern Illinois University for providing complete line listings for bromobenzene. The hemispherical resonators were polished and mounted in the vacuum chamber by Mr. Kurt Weihe and Mr. Bobby Turner of the Physics Department machine shop at the University of North Texas. Bromobenzene and iodobenzene were kindly donated by Professors Michael Richmond and Trent Selby, respectively, both at the University of North Texas Department of Chemistry. This research has been financially supported by the University of North Texas through start up funding and a Junior Faculty Summer Research Fellowship and by the Petroleum Research Fund (type G), administered by the American Chemical Society. We gratefully acknowledge financial support from two Faculty Research Grants from the University of North Texas, and a Ralph E. Powe Junior Faculty Enhancement Award administered by Oak Ridge Associated Universities, and a Faculty Research Grant from the University of North Texas. We thank Professor James Marshall, at the University of North Texas, for providing a sample of thorium metal.

TABLE OF CONTENTS

LIST OF TABLES

LIST OF FIGURES

CHAPTER 1[1]

A FABRY–PERÓT TYPE RESONATOR TUNABLE BELOW 2 GHZ FOR USE IN TIME DOMAIN ROTATIONAL SPECTROSCOPY: APPLICATION TO THE MEASUREMENT OF THE RADIO FREQUENCY SPECTRA OF BROMOBENZENE AND IODOBENZENE

1.1 Introduction

Since its invention by Balle and Flygare the cavity pulsed Fourier transform microwave spectrometer with pulsed nozzle particle source[1] has provided high resolution spectra allowing insights into a variety of problems in the physical sciences. Spectral features spaced by as little as 20 kHz can easily be resolved and the technique is particularly powerful in the study of transient or short-lived species. The basic design of the instrument has seen many improvements over the last 25 years (see for example references 2 and 3) including extension of the frequency range to 140 GHz[4]. Indeed, attempts are underway to extend the principle of the "Balle–Flygare" into the terahertz region[5]. With two exceptions there has been little effort to extend the frequency range in the other direction, into the radio frequency region. A survey of the literature demonstrates that most spectrometers do not operate below 2 GHz and many cavity FTMW spectroscopists are limited to make measurements above 5–6 GHz.

With regard to the two exceptions the first involved the study of the rotational spectra of rare gas–benzene–water trimers by Arunan et al.[6]. In this work, a rotational

[1] This entire chapter is reproduced from Etchison, K. C.; Dewberry, C. T.; Kerr, K. E.; Shoup, D. W.; Cooke, S. A., A Fabry–Perót type resonator tunable below 2 GHz for use in time domain rotational spectroscopy: Application to the measurement of the radio frequency spectra of bromobenzene and iodobenzene Journal of Molecular Spectroscopy 2007, 242 (1), 39-45, with permission from Elsevier.

transition was recorded at 1888.7580 MHz. This was achieved using a traditional Balle–Flygare spectrometer "stretched" beyond its lower limit of 2 GHz by using a balanced ¼ wavelength antenna and by placing "collars" around the edges of the mirrors to prevent losses due to the large microwave beam waist. It was not determined whether the instrument could operate below 1.8 GHz but the authors' note that most of the microwave circuit components were operating well outside their design limits. In the second exception a molecular beam Fourier transform microwave spectrometer operating in the range of 1–4 GHz has been designed by Storm et al.[7]. In this very well constructed instrument, a cylindrical resonator for use in the TE_{01} mode was used. This is in contrast to the TEM_{00q} modes employed in the Balle–Flygare Fourier transform microwave spectrometer. The cylindrical resonator was chosen to avoid having to deal with very large mirror radii, however, we show below that large mirror radii may be offset by increasing the radius of curvature. We also note that in this instrument several sets of antenna were required to cover the complete 1–4 GHz range where as we have been able to obtain complete coverage with a single set of antenna. The lowest frequency transition presented by Storm et al. is at 1323.7282 MHz for the 1-azabicyclo [2,2,2] octane–H_2S complex.

With regard to the need for a low frequency instrument it should be noted that spectroscopists have developed many ways of placing chemicals with low volatility into the gas phase. These methods have made large organic molecules and heavy, transition metal-containing complexes available for spectroscopic investigation. Many of these methods have been incorporated into cavity based FTMW spectroscopy (see for

example references 8, 9, 10, 11, & 12). Using these techniques rotational spectroscopists are targeting larger molecules than have ever previously been attempted. Along with large molecular size and the inclusion of heavier elements come smaller rotational constants. In consequence, low J rotational transitions, which can often be the most informative, fall at the low frequency end of the spectral region traditionally surveyed. For this reason extending the frequency range of the traditional Balle–Flygare experiment into the radio frequency region is a worthwhile endeavor. Many problems surround the observation of molecular transitions in the radio frequency region. One significant problem concerns the lack of sufficiently large population differences necessary for observation of a molecular transition. A very clever method of overcoming this problem has been presented by Wötzel et al.[13] and involves the use of "borrowing" population differences through a double resonance technique. This technique has enabled radio frequency transitions as low as 7 MHz to be observed with very good accuracy for ethyl fluoride. The technique does however require the use of a sample cell meaning transient species are less convenient for study. Also the use of a double resonance technique does not permit the observation of low J transitions.

A cavity based instrument in which target molecules undergo a rapid cooling via an adiabatic expansion from a pulsed molecular source will overcome these problems. However, new problems arise in the design of a radio frequency cavity[14, 15]. In this paper, we address these problems. To our knowledge manufacturing a cost effective, reasonably sized cavity with a high Q value that may be successfully tuned below 2 GHz has not previously been reported. In this paper, we present the design and construction

of such a cavity and present results in which the lowest $\Delta J = +1$ transitions, falling as low as 1.1 GHz; have been recorded for both bromobenzene and iodobenzene.

1.2 Experiments

1.2.1 Resonator Design

The frequency of operation of a cavity formed from two mirrors depends upon their geometry. Spherical, concave mirrors are generally used in FTMW spectroscopy. The radius of curvature for these mirrors may be found by making the Fresnel number, N, unity for the lowest frequency (longest wavelength) of interest according to the equation:

$$\frac{a^2}{R\lambda} = \mathrm{N} \qquad (1)$$

Here a is the mirror radius, R is the radius of curvature and λ is the wavelength. The original Balle–Flygare spectrometer[1] had mirrors with radii of 177.8 mm and radii of curvature of 840 mm. This design leads to an optimum frequency region of ~8 GHz. In fact, the instrument is reported as operating to a lower frequency limit of 4.5 GHz.

Clearly to access long wavelengths one requires the mirrors to have large radii and/or small radii of curvature. In the vacuum chamber available to us at the University of North Texas the largest radius that could be considered was ~200 mm (~8 in.). The smallest radius of curvature that can be conceived is to construct the mirrors to be hemispherical i.e., the radius of curvature should equal the mirror radius. Concerns had previously been raised about highly curved mirrors causing distortion of the

wavefront[14]. In this work, we demonstrate that this is not a prohibitive factor when performing rotational spectroscopy.

Suitable, albeit low quality, hemispheres were found commercially available from AMS industries, Ltd. These hemispheres have a variety of end uses including use as "pigs" in the oil industry, as camera housings for stunt photography in the motion picture industry and also for general artistic constructions. The hemispheres are constructed from 6061 grade aluminum and are produced through a spinning process. The consequence of this process is that the interior finish of the hemispheres displays numerous surface defects. The hemispheres also have a one-inch diameter hole at their center that is used to hold them on the tool during the machining process. This hole was filled by the welding of an aluminum plug. The mirrors were then polished in a lathe over a period of 8 h starting with coarse sandpapers and steadily progressing to a fine grade polishing fluid. When complete the mirror surface defects remained as high as 2–3 mm. Given the wavelengths of interest are in the 200 mm region or higher, it was anticipated that these defects would not pose a significant problem. However, clearly improvements may be made by machining the mirrors using higher quality techniques.

The finished mirrors have radii and radii of curvature of 203.2 mm. Eq. (1) indicates that these mirrors have an optimum frequency region of ~1.5 GHz. It is demonstrated below that it is possible to go to frequencies lower than this. A photograph of the mirrors is shown in Figure 1.

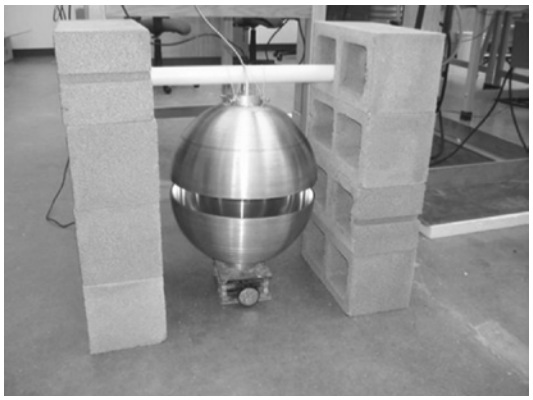

Figure 1. Photo of cavity undergoing testing prior to being positioned within the vacuum chamber.

The mirrors have been mounted onto a rail. One is stationary and the other may be moved to enable tuning of the cavity to a given frequency. The movable mirror has a travel of ~150 mm.

1.2.2 Q Factor

The Q factor of a resonator may be crudely approximated by:

$$Q = \frac{\text{resonant frequency}}{\text{spectral width of the mode}} \tag{2}$$

Clearly, to achieve high Q factors at low frequencies very narrow modes must be achieved. In our resonator, the spectral widths of the modes are consistently on the same order of magnitude as those achieved in higher frequency resonators, i.e. ≈1–2 MHz. However, this results in a small Q, ~200 ??, at the lowest frequencies accessible. This Q is almost two orders of magnitude smaller than that found for higher frequency resonators. Diffraction losses are certainly a problem at very low frequencies. These losses are discussed more fully in regards to the resonator's stability below in the resonator stability section.

It is apparent from experiment that this Q is high enough to successfully perform time domain rotational spectroscopy. Again, reducing surface defects, using more highly

conducting materials such as niobium[16] and possibly cooling to liquid nitrogen temperatures[3, 16] are all likely to improve the resonator's performance. We note that quite high Q factors, ~5000, are available at higher frequencies. This is also born out in experiment where OCS transitions falling above 12 GHz have easily been observed.

In keeping with higher frequency instruments electromagnetic fields are coupled in and out of the cavity using ¼ wavelength antenna. The two antennae (one for transmission and one for reception) are located on the same mirror. The length of the antenna (80 mm) together with the curvature of the mirror means that the antennae are required to be bent at an angle of ~100° compared to the more traditional right angled antenna. This coupling method is far from ideal placing a large load on the resonator.

1.2.3 Resonator Stability

Traditionally a stable, open resonator is one in which resonant modes are narrowly confined along the resonator axis. Diffraction losses of these modes, i.e. the energy losses due to leakage out the sides of the resonator or past the edges of the mirrors, are small. Conversely an unstable cavity is one in which energy losses due to diffraction are large. A mode chart may be constructed to illustrate a quantitative relation between the resonators geometry and its stability. In the case where the resonator is formed from two identical mirrors the boundaries to the stable regions are given by equation 3 (see reference 3 and references therein):

$$0 \leq g^2 \leq 1 \qquad (3)$$

where

$$g = 1 - \frac{d}{R} \tag{4}$$

where d is the distance between the centers of the mirrors and R is the radius of curvature of each mirror. For our resonator, when the mirrors are as close together as geometrically possible, d = 2R and therefore g = ~1. The conditional expression above indicates that the resonator is on the edge of "stability". As the mirrors are moved apart the suggestion is that the resonator becomes increasingly unstable[17, 18, 19].

A closer look at the above equation indicates that the application of this treatment to the resonator used in this work is unsatisfactory. The g-parameter has no dependence on a mirrors radius. Implicit to the idea of stability, as defined above, are the assumptions that (a) the mirror radius is large and that (b) the radius of curvature is significantly larger than the mirror radius[20]. This second assumption is not valid in the present case.

In order to determine whether the hemispherical mirrors give improved performance at low frequencies an experiment was conducted. Two polished, aluminum mirrors with radius of curvature of 384 mm and radii of 140 mm were placed inside the vacuum chamber. These mirrors have been successfully used in the measurement of rotational spectra at frequencies from 5 to 26 GHz. At all times during this experiment, the distance between the mirrors was within stable limits according to the conditional expression above. With these mirrors, resonant modes were so extremely broad below 2 GHz that (i) satisfactory tuning of the resonator was not possible and (ii) the Q factor was not determinable but obviously very small. It is evident that diffraction losses

prohibit the use of this open resonator at low frequencies. Larger mirrors would give improved results. However, we note in experiments conducted by Ahmed and Auchterlonie, using mirrors with radii of 500 mm and radii of curvature of 10000 mm, that at 3 GHz the beam extended transversely over the entire 1000 mm mirror diameter[14].

In comparison, diffraction losses are small for the hemispherical mirrors used in this work. The probable, and perhaps obvious, reason for this is that the hemispherical mirrors contain the low frequency modes better than more open mirrors. We suggest that our arrangement is probably better considered a "nearly closed" resonator as opposed to an "open" resonator.

Phenomenologically, we may state that low frequency rotational spectra have been collected using relatively compact mirrors. Improvements can be made. Further experiments are underway to fully characterize the field distribution and losses of our resonator.

1.2.4 Pulsed Nozzle Source

A solenoid valve (Series 9, Parker–Hannifin™) has been mounted in the center of the stationary resonator. This allows the molecules to expand coaxially to the direction in which the radiation is propagated into the chamber. This coaxial arrangement has been demonstrated to provide higher resolution compared to a perpendicular nozzle orientation[2]. Usually this configuration results in all spectral features being observed as

doublets due to the Doppler effect. However we find that the Doppler doubling, which decreases as a function of frequency, is not resolvable below ~2 GHz.

Bromobenzene or iodobenzene were pulsed into the cavity by bubbling the argon backing gas through a 1–2 mL sample of the liquid. Transitions above ~3 GHz could easily be seen by keeping the argon backing pressure at 1–1.5 bar. For the lowest frequency transitions greater intensities could be obtained by increasing the backing gas pressures to 7–8 bar. Clearly the increased backing pressure has the effect of further cooling the gas as it expands between the resonators allowing the populations of the very lowest rotational levels to increase. It is likely that even greater cooling may be achieved with backing gases other than argon however we have not attempted such experiments. The vacuum chamber was held at a pressure of $\sim 10^{-5}$ torr and pumping speeds were sufficient to allow 10 nozzle pulses per second.

1.2.5 Radio Frequency Circuit

The circuit constructed follows closely the designs outlined by Grabow et al.[2-3] with the obvious exception that all the electronic components are rated for operation in the radio frequency (RF) region. The instrument is controlled centrally by a PC running software written by Jens-Uwe Grabow[21]. The circuit is presented in Figure 2. It should be noted that radio frequency components are commercially available with similar or higher specifications than those traditionally used in microwave spectroscopy and often at considerably less cost.

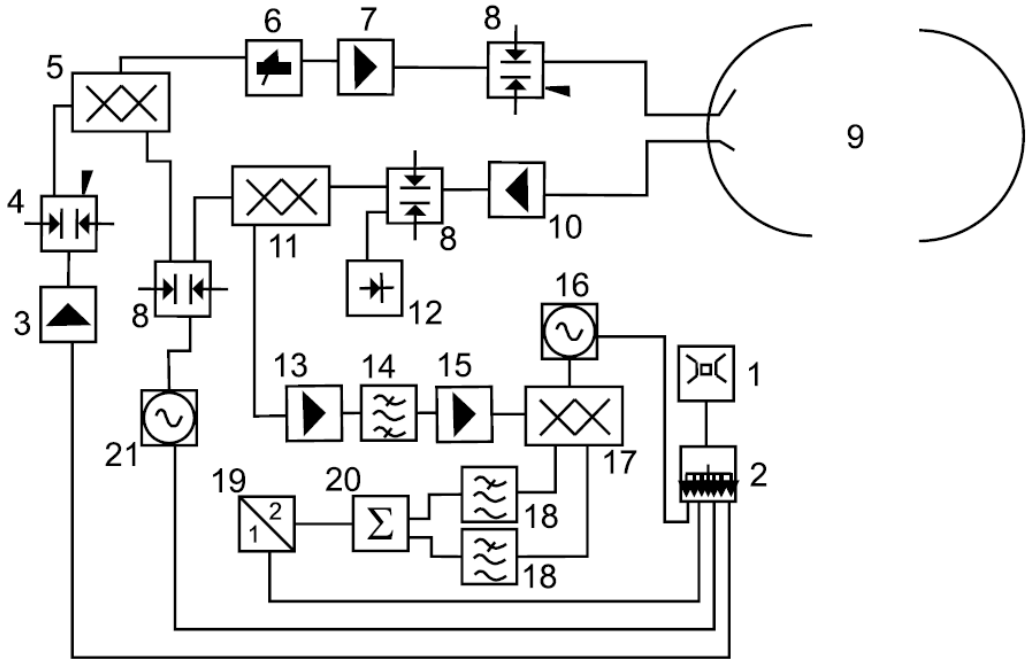

Figure 2. A schematic of the radio frequency circuit used in the experiments.

1. Hewlett Packard (HP) 5061A Cesium beam frequency standard. 2. Low Noise Distribution Amplifier, Wenzel Associates LNDA2-10-2-2-BNC. 3. RF voltage gain control amplifier, Minicircuits ZFL-1000GH. 4. RF SPDT switch Minicircuits ZYSW-2-50-DR. 5. Single-sideband modulator (SSB) (a) 300– 1000 MHz, 10 MHz ±1 MHz Intermittent Frequency (IF), Polyphase Microwave SSB0310X (b) 750–2200 MHz, 10 MHz ±1 MHz IF, Polyphase Microwave SSB0722A. 6. Attenuator assembly (a) HP 84904K, 11 dB (b) HP 84907K, 70 dB. 7. MW Power Amplifier, HP 83017A. 8. Single pulse double throw (SPDT) switch, Sierra Microwave Technology SFD0526-001. 9. Cavity. 10. Low noise amplifier, Lucix S001040L4501 (gain 45 dB, noise figure of 1.5dB). 11. Image rejection mixer (a) 300–1000 MHz, 10 MHz ±1 MHz IF, Polyphase Microwave IRM0310X (b) 700–2200 MHz, 10 MHz ±1 MHz IF, Polyphase Microwave IRM0722A. 12. Diode detector, HP 8473C. 13. RF low noise amplifier, Minicircuits ZFL-1000LN. 14. 10 MHz Bandpass filter, KR Electronics, Inc. 2588. 15. RF voltage gain amplifier, Minicircuits ZFL-1000G. 16. RF synthesizer, HP 8656B. 17. In-phase Quadrature (I/Q) Demodulator, Minicircuits MIQC-60WD. 18. RF low pass filters, Minicircuits SLP-5. 19. 10 MHz doubler, Wenzel Associates, LNHD–10-13. 20. Personal computer. 21. Microwave (MW) synthesizer, HP 8340B.

1.3 Results

The microwave spectra of bromobenzene has previously been recorded most recently by Peebles et al.[22]. These authors have used a Balle–Flygare spectrometer to record transitions at high resolution above 7 GHz. The microwave spectra of iodobenzene has also already been recorded by Caminati[23] using a waveguide spectrometer in the frequency region of 12–26 GHz. For bromobenzene B + C = 1841

MHz and for iodobenzene B + C = 1412 MHz. The $^{a}R_{01}$ rotational transitions are spaced by approximately (B + C) and large hyperfine splittings occur due to the coupling of the ^{79}Br, ^{81}Br and I nuclear spins with the molecular angular momentum. Both molecules have relatively large dipole moments (1.5 D and 1.4 D, respectively[24]) are easily available and do not need to be heated in order for their spectra to be observed. For these reasons these molecules were considered ideal candidates for the testing of our experiment.

Given that bromobenzene has already been studied at high resolution only the lowest R branch transitions for each bromine isotope were recorded and then the effect these measurements had on the overall quality of the fit were observed. For iodobenzene an attempt was made to measure as many transitions as possible. This was necessary because the rotational constants of iodobenzene were not sufficiently well determined to permit the lowest frequency transitions to be located immediately. The lowest frequency transition so far recorded with this instrument, the iodobenzene $J_{K-1K+1} = 1_{01} - 0_{00}$, F = 5/2–5/2 transition at 1130.5 MHz, is shown in Figure. 3.

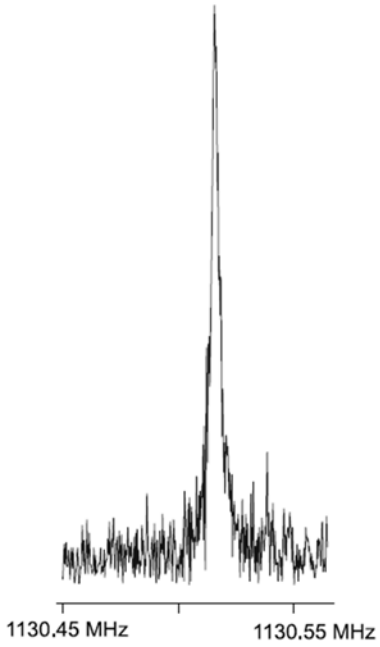

Figure 3. Power spectrum of the $J_{K-1K+1} = 1_{01} - 0_{00}$, F = 5/2–5/2 transition for iodobenzene.

The experiment required 30,000 averaging cycles and is shown as a 4k transform. This is the lowest recorded transition with this instrument so far. The line width is 7 kHz (FWHM).

The line width is 7 kHz (FWHM). Further, illustrative portions of spectra are given in Figures 4–6. A complete listing of all the frequencies measured is given in Table 1 for bromobenzene and Table 2 for iodobenzene. Spectra were fit using the SPFIT program[25] and the resulting constants are presented in Table 3 for bromobenzene and Table 4 for iodobenzene. For bromobenzene the line frequencies of Peebles et al.[22] were used in the fit. For iodobenzene only those frequencies given in Table 2 were used.

Table 1
Observed and Calculated Hyperfine Transition Frequencies for the $J'_{K-1K+1} = 1_{01} - 0_{00}$ Rotational Transitions for Two Isotopomers of Bromobenzene

Isotopomer	F' - F"	Frequency (MHz)	Obs–calc (kHz)[a]
^{79}Bromobenzene	1/2 - 3/2	1705.4928	-1.7
	5/2 - 3/2	1814.8292	8.5
	3/2 - 3/2	1955.2233	-3.4
^{81}Bromobenzene	1/2 - 3/2	1709.7843	-4.9
	5/2 - 3/2	1801.396	11.2
	3/2 - 3/2	1918.5128	-1.3

[a] Observed–calculated residuals (kHz).

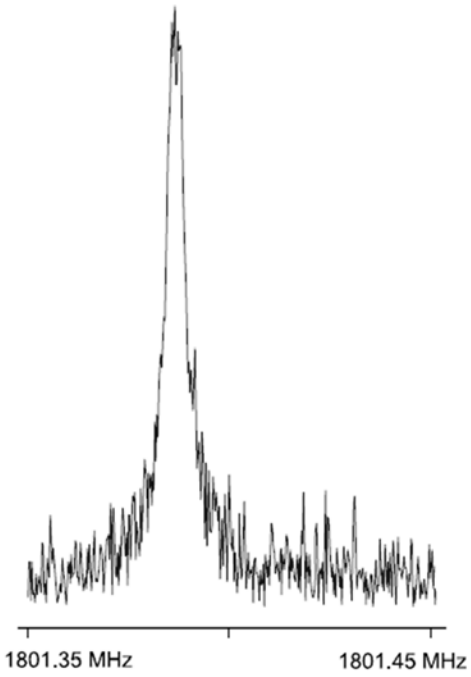

Figure 4. The $J_{K-1K+1} = 1_{01} - 0_{00}$, F = 5/2–3/2 transition for bromobenzene.

The experiment required 4900 averaging cycles and is shown as a 4k transform (no zero filling).

Table 2
Observed and Calculated Transition Frequencies for Iodobenzene

J'_{K-1K+1} - J''_{K-1K+1}	F' - F"	Frequency (MHz)	Obs–calc (kHz)[a]
1_{01} - 0_{00}	5/2 - 5/2	1130.5292	-1.1
	7/2 - 5/2	1522.7417	3.7
	3/2 - 5/2	1705.5086	-13.2
2_{12} - 1_{11}	7/2 - 5/2	2505.6513	5.7
	5/2 - 5/2	2540.2865	-2.8
	9/2 - 7/2	2866.7556	5.2
2_{11} - 1_{10}	7/2 - 5/2	2682.1584	4.5
	5/2 - 5/2	2719.6122	-4.1
	9/2 - 7/2	3044.9135	4.4
2_{02} - 1_{01}	3/2 - 3/2	2696.9154	-4.2
	9/2 - 7/2	2871.2164	10
3_{22} - 2_{21}	7/2 - 7/2	4005.2937	-4.4
3_{13} - 2_{12}	7/2 - 5/2	4034.0946	-1.7
	9/2 - 7/2	4066.8074	3.9
	7/2 - 7/2	4068.7303	-9.7
3_{03} - 2_{02}	3/2 - 1/2	4066.9094	-2.6
8_{08} - 7_{07}	21/2 - 19/2	11212.6685	3.5
8_{27} - 7_{26}	21/2 - 19/2	11303.9183	4.7
9_{19} - 8_{18}	21/2 - 19/2	12296.2667	-3.8
	23/2 - 21/2	12296.286	5.7
9_{09} - 8_{08}	23/2 - 21/2	12584.9237	-4.1
9_{28} - 8_{27}	23/2 - 21/2	12706.7599	-1.2
9_{27} - 8_{26}	21/2 - 19/2	12833.6848	-2.1

[a] Observed–calculated residuals (kHz).

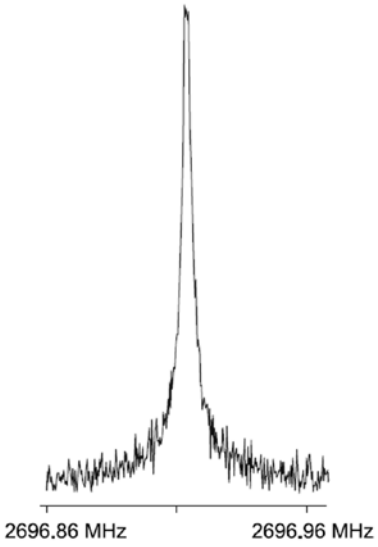

Figure 5. The $J_{K-1K+1} = 2_{02}–1_{01}$, F = 5/2–5/2 transition for iodobenzene.

The experiment required 5000 averaging cycles and is shown as a 4k transform.

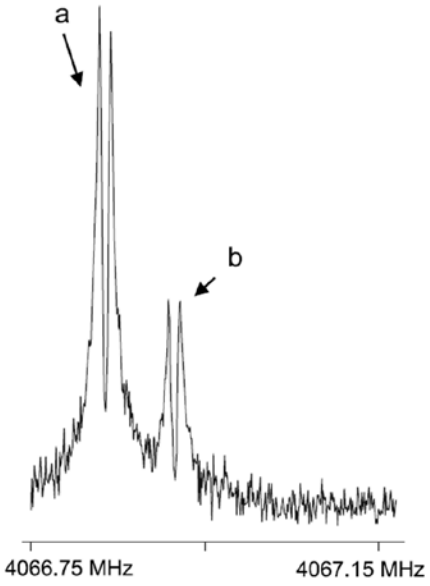

Figure 6. Two transitions for iodobenzene.

(a) The $J_{K\text{-}1K+1} = 3_{13} - 2_{12}$, F = 9/2–7/2 transition for iodobenzene.
(b) The $J_{K\text{-}1K+1} = 3_{03}–2_{02}$, F = 3/2–1/2 transition for iodobenzene. The experiment required 550 averaging cycles and is shown as a 4k transform.

1.4 Discussion

Table 3 compares two fits for ^{79}bromobenzene. In one fit the transitions recorded in Table 1 are combined with those recorded in reference 22. The second fit neglects the transitions in Table 1 simply reproducing the fit of reference 22. Although little overall improvement may be noted the measurement of the lowest $\Delta J + 1$ transitions for bromobenzene do clearly reduce the uncertainty in the nuclear quadrupole coupling constant for bromine by about 30% compared to the use of the higher frequency transitions alone. This is easily understood on the basis that hyperfine structure caused by the coupling of nuclear quadrupole moments to the angular momentum of the molecule has the largest frequency spread for the lowest J transitions.

Table 3
Spectroscopic Parameters for ^{79}Bromobenzene

Spectroscopic constant	This work[a]	Literature[b]
A (MHz)	5667.749(52)	5667.750(52)
B (MHz)	994.9018(2)	994.9018(2)
C (MHz)	846.2567(2)	846.2567(2)
ΔJ (kHz)	0.0252(23)	0.0251(24)
ΔJK (kHz)	0.193(21)	0.191(21)
χaa (MHz)	556.689(10)	556.700(16)
(χbb - χcc) MHz	-29.031(104)	-29.020(104)

[a]These results have been obtained by fitting the transitions recorded in[22] together with those extra lines given in Table 1. Numbers in parentheses show one standard deviation in units of the last significant figure.
[b]Ref[22]

Table 4
Spectroscopic Parameters for Iodobenzene

Spectroscopic constant	This work[a]	Literature
A (MHz)	5669.33(15)	5671.89(73)
B (MHz)	750.4135(56)	750.416(2)
C (MHz)	662.63698(42)	662.627(1)
ΔJ (kHz)	0.0170(19)	Not reported
ΔJK (kHz)	0.137(82)	Not reported
χaa (MHz)	-1892.063(12)	-1892.1(2.2)
(χbb - χcc) MHz	65.659(65)	60.3(5.2)

[a]These results have been obtained by fitting to only those transitions given in Table 2. Numbers in parentheses show one standard deviation in units of the least significant figure.

The reduced uncertainty is of little interest in the present case however this result is of considerable significance for the future study of large molecules containing quadrupolar nuclei with significantly smaller moments such as deuterium, nitrogen and chlorine. For large molecules, where hyperfine structure arising from these nuclei is anticipated, a low frequency spectrometer such as this one will be a necessity when probing electronic structures.

Advantages are also clear from the recorded transitions of iodobenzene. Using the SPCAT program[25] it is possible to predict all of the allowed rotational transitions for iodobenzene with an intensity greater than $\log_{10}$ - 3.0 nm^2 MHz. Assuming a rotational temperature of 4K and considering only a-type transitions 51 pure rotational transitions were predicted to fall in the 1–4 GHz region. This should be compared to the 304 rotational transitions predicted to fall in the 9– 12 GHz region. Clearly an advantage in regard to assignment is available by working in the less congested lower frequency region.

1.5 Conclusion

A Fabry-Perót type cavity has been designed, constructed and implemented which when incorporated into a Balle–Flygare type spectrometer is useful in the recording of pure rotational spectra in the radio frequency region. The system has reasonable sensitivity and has easily recorded spectral transitions as low as 1.1 GHz. The usefulness of the instrument has been demonstrated by recording the lowest ΔJ = +1 transitions for bromobenzene and iodobenzene. For bromobenzene a decrease in uncertainty in the nuclear quadrupole-coupling constant of bromine has been obtained. There is anticipation that this type of cavity, when incorporated into a Balle–Flygare type spectrometer, will greatly aid the study of large and/or heavy molecules by enabling less dense regions of spectra to be accessed. Experiments are underway to determine the lower frequency limit of the spectrometer. The cavity is tunable to a lower limit of 534 MHz.

CHAPTER 2[2]

BORN–OPPENHEIMER BREAKDOWN EFFECTS AND HYPERFINE STRUCTURE IN THE ROTATIONAL SPECTRUM OF STRONTIUM MONOSULFIDE, SRS

2.1 Introduction

Two previous high-resolution spectroscopic studies have been performed on strontium sulfide. The first study by Pianalto et al.[26] reports the study of the $A^1\Sigma^+$–$X^1\Sigma^+$ transition. The spectrum was observed at sufficiently high resolution to allow a rotational analysis. Only the most abundant SrS isotopomer, $^{88}Sr^{32}S$, was observed. The second study, by Halfen et al.,[27] was primarily a study of the SrSH molecule using pure rotational spectroscopy in the millimeter wave region; several rotational transitions from $^{88}Sr^{32}S$ were observed and reported.

In this work Fourier transform microwave spectroscopy has been used to record the pure rotational spectra of four isotopomers of SrS between 6 and 26 GHz. Besides improving the precision of previously reported molecular constants our interest in this molecule is twofold. First, we seek to determine the hyperfine constants for the $^{87}Sr^{32}S$ isotopomer. Second, the first observations of pure rotational transitions from minor SrS isotopomers will allow evaluation of Born–Oppenheimer breakdown parameters for the molecule. These two goals have been successfully achieved and the results reported below.

[2] This entire chapter is reproduced from Etchison, K. C.; Dewberry, C. T.; Cooke, S. A., Born-Oppenheimer breakdown effects and hyperfine structure in the rotational spectrum of strontium monosulfide, SrS. Chemical Physics 2007, 342 (1-3), 71-77, with permission from Elsevier.

2.2 Experiment

We have constructed a new Balle–Flygare-type Fourier transform microwave spectrometer at the University of North Texas. The instrument closely follows the coaxially oriented beam resonator arrangement (COBRA) as presented by Grabow et al.[2]. Small differences exist in the microwave circuit of the instrument.

A schematic of the circuit is given in Figure 7. Several features are notable. First, the modulated circuit uses an intermediate frequency of 30 MHz and covers 6–26 GHz without the need to change any components. Second, in an effort to reduce the noise figure of the instrument the low noise amplifiers have been placed as close to the receiving, L-shaped antenna as possible. In the configuration used in this experiment it was necessary to place the amplifiers inside the vacuum chamber and cooling them with a cold-water loop. Further to the circuit the instrument is equipped with a "Walker–Gerry"-style laser ablation nozzle[10]. This allows the study of metal-containing compounds and other species of low volatility.

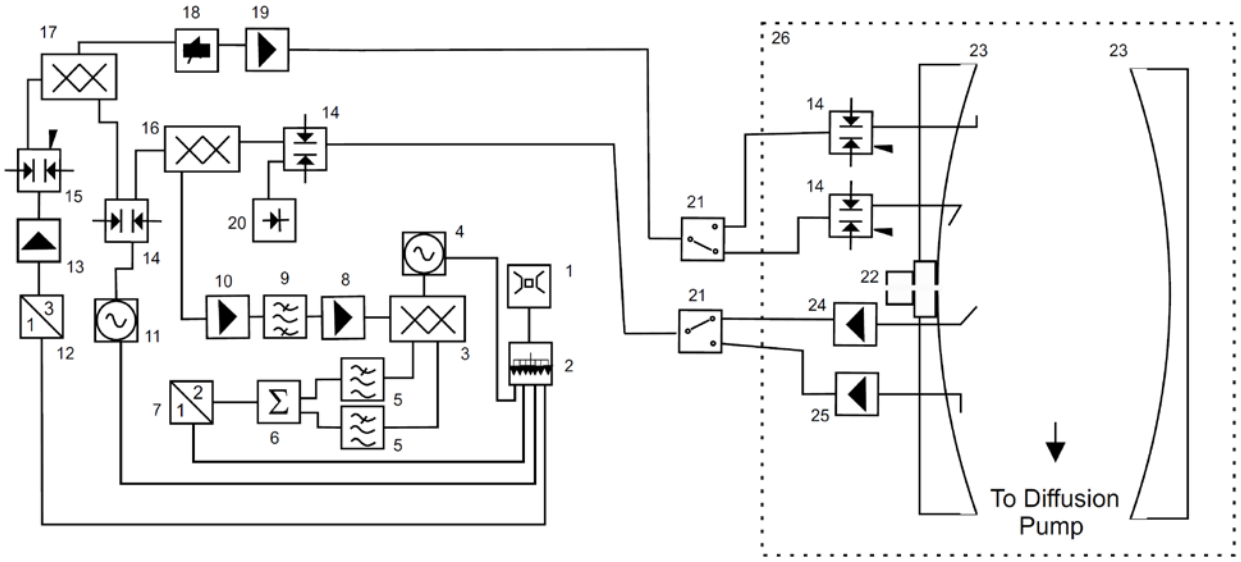

Figure 7. Schematic of the Fourier transform microwave spectrometer.

(1) HP 5016A cesium beam frequency standard, (2) 10 MHz distribution amplifier, Wenzel Associates 600-15888, (3) I/Q Demodulator, Minicircuits MIQC-60WD, (4) RF Synthesizer HP 8656B. 1–990 MHz, (5) low pass filter, Minicircuits SLP-5, (6) personnal computer, (7) 10 MHz Doubler, Wenzel Associates, LNHD-10-13, (8) amplifier,Minicircuits ZFL-1000G, (9) 30.5 MHz band pass filter, Reactel 3B4-30.5-1 S11, (10) low noise amplifier, 1–500 MHz, Miteq AU-2A-015, (11) MWsynthesizer, HP 8340B 0.01–26.5 GHz, (12) 10 MHz tripler, Wenzel Associates, LNOM-10-3-13-13-BM-BM, (13) amplifier, Minicircuits ZFL-1000GH,(14) SPDT pin diode switch, Sierria Microwave Technology, SFD0526, (15) SPDT pin diode switch, Minicircuits ZYSW-2-50DR, (16) image rejection mixer, Miteq, IRM0226LC1, (17) single sideband upconvertor, Miteq, SM0226LC1M, (18) attenuator chain, HP 84904K 11 dB, HP 84907K 70 dB, (19) power amplifier, HP 83017A, (20) MW detector HP 8474C, (21) MW relay HP 8762C, (22) Solenoid Valve, Series 9 Parker Hannifin, (23) aluminum resonators, (24) low noise amplifier, Miteq, JS4-06001800-145-10A, 6–18 GHz, (25) low noise amplifier, Miteq, AMF-5S-180260-45, 18–26 GHz, (26) Vacuum Chamber.

Briefly, the instrument is operated in the following way. Our microwave cavity is formed from two opposing, spherical, aluminum mirrors. One of these mirrors is held stationary while the other may be moved with micrometer resolution using a stepper motor. The cavity is tuned to be in resonance with a chosen microwave frequency. Samples, entrained in a noble gas, are supersonically expanded in to the cavity from the laser ablation nozzle located at the center of the fixed mirror. Accordingly, all observed lines appear as Doppler doublets as the propagation of microwaves occurs coaxially to the direction of the pulsed molecular jet. Line frequencies are determined

by taking the average of the Doppler components. Measurements recorded with our instrument have an estimated uncertainty of less than 1 kHz.

In contrast to the two prior studies on SrS in this work, the species has been prepared by reacting laser ablated Sr atoms with OCS. A small lump of Sr metal was placed on a support and rotated and translated within the ablation nozzle. Pulses of radiation from a Nd:YAG laser (New Wave Minilase II, k = 1064 nm) were focused on to the target rod. Coinciding with the ablation event a pulse of gas (0.1% OCS in a 30:70 He:Ne gas mix) was pulsed into the Sr ablated metal and the products injected into the microwave cavity. The backing pressure of the gas was 7 atm. Initially H_2S was used as the precursor gas but SrS signals were very weak compared to the use of the OCS precursor.

2.3 Results and Analysis

2.3.1 Analyses of the Spectra

Using the SrS constants of Halfen et al.[27] transitions for the $^{88}Sr^{32}S$ isotopomer were located immediately. A sample transition is given in Figure 8.

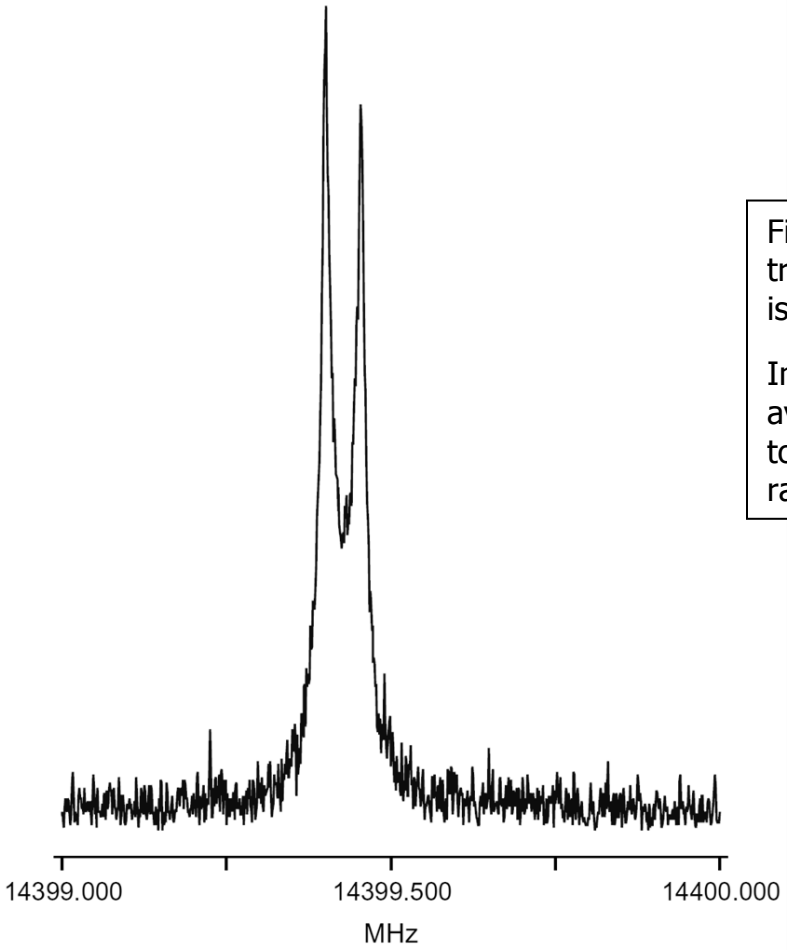

Figure 8. The J = 2-1, v =1 transition for the $^{88}Sr^{32}S$ isotopomer.

In this experiment 100 averaging cycles were required to achieve this signal to noise ratio.

Lines for the remaining isotopomers could easily be predicted from these transitions within an accuracy of a few hundred kilohertz. The data collected are presented in Table 5.

Table 5
Measured Transition Frequencies for SrS

Isotopomer	J'–J''	F'–F''	v	Frequency (MHz)		obs-calc (kHz)[b]
				Hyperfine splitting	Line center[a]	
$^{88}Sr^{32}S$	1–0		0		7228.4416	1.1
	1–0		1		7199.7328	2.0
	1–0		2		7170.8786	1.2
	2–1		0		14456.8478	0.6
	2–1		1		14399.4278	0.2
	2–1		2		14341.6974	-1.6
	2–1		3		14284.7379	0.0
	3–2		0		21685.1893	2.8
	3–2		1		21599.0599	-0.9
	3–2		2		21512.4599	-3.6
$^{87}Sr^{32}S$	2–1	11/2-9/2	0	14502.1144		-0.4
	2–1	13/2-11/2	0	14501.4882	14501.0188[c]	
	2–1	5/2-7/2	0	14501.8850		
	3–2	15/2-13/2	0	21751.7078		-2.8
	3–2	9/2-9/2	0	21751.9348	21751.4467[c]	
	3–2	13/2-11/2	0	21752.0567		
$^{86}Sr^{32}S$	2–1		0		14546.3569	1.4
	2–1		1		14488.3995	0.5
	3–2		0		21819.4495	1.5
$^{88}Sr^{34}S$	3–2		0		20751.8549	0.0

[a]These are measured line frequencies except for $^{87}Sr^{32}S$, for which they are the hypothetical unsplit line frequencies with hyperfine structure removed.

[b]These residuals are those of the Dubham fits (results in Tables 7 and 8).

[c]Unsplit transition frequencies with hyperfine structure removed.

Transitions observed included the J = 1–0, J = 2–1 and J = 3–2 transitions. For the most abundant isotopomer rotational transitions within the v = 0, 1, 2 and 3 states were observed. In total four isotopomers were studied; $^{88}Sr^{32}S$, $^{87}Sr^{32}S$, $^{86}Sr^{32}S$ and $^{88}Sr^{34}S$. Analyses of these data began with the $^{87}Sr^{32}S$ isotopomer. The ^{87}Sr isotope has a non-zero nuclear spin, I = 9/2. The coupling scheme $F = J + I_{Sr}$ was employed and

the spectra interpreted in terms of the following Hamiltonian:

$$\mathbf{H} = \mathbf{H}_{\text{rot}} + \mathbf{H}_{\text{elec quad}}, \quad (5)$$

where

$$\mathbf{H}_{\text{rot}} = B_v J^2 - D_J J^4, \text{ and}$$

$$\mathbf{H}_{\text{elec quad}} = -\frac{\mathbf{1}}{\mathbf{6}} \left(\mathbf{V}_{\mathbf{Sr}}^{(\mathbf{2})} \cdot \mathbf{Q}_{\mathbf{Sr}}^{(\mathbf{2})}\right)$$

Neither a nuclear spin-rotation term, nor any other terms, was required for a satisfactory fit. Line frequencies were fitted using Pickett's weighted least-squares program SPFIT[25]. The determined constants for the $^{87}Sr^{32}S$ isotopomer are given in Table 6.

Table 6
Spectroscopic Constants for $^{87}Sr^{32}S$

Constant	Value/MHz
B_0	3625.2656(13)[a]
D_0	0.00136(6)
eQq(^{87}Sr)	-21.959(85)

[a]Numbers in parentheses are one standard deviation in units of the last significant figure.

Having dealt with the only isotopomer exhibiting hyperfine structure, a Dunham-type, multi-iostopomer analysis[28] was pursued for the remaining isotopomers. The $^{87}Sr^{32}S$ data could be included in this fitting procedure by using the rotational and centrifugal distortion constants from Table 6 to predict hypothetical, unsplit line frequencies for this isotopomer. These frequencies, given in Table 5, could then be used in the multi-isotopomer analysis.

The following equations are used in the multi-isoptopomer analysis:

$$E(v, J) = \sum_{k,l} Y_{kl} \left(v + \frac{1}{2}\right)^k [J(J+1)]^l \quad (6)$$

To the accuracy of the present work, excepting Y_{01}, each $Y_{kl} = U_{kl}\mu^{-(k+2l)/2}$, where U_{kl} is the mass independent Dunham parameter. The Y_{01} term contains contributions from both adiabatic and non-adiabatic effects. The term Y_{01} is given by

$$Y_{01} = \frac{U_{01}}{\mu}\left[1 + m_e\left(\frac{\Delta_{01}^{Sr}}{M_{Sr}} + \frac{\Delta_{01}^{S}}{M_S}\right)\right] \quad (7)$$

where μ is the reduced mass of the molecule, m_e is the mass of the electron, Δ_{01}^{Sr} and Δ_{01}^{S} are the Born–Oppenheimer breakdown (BOB) terms, and M_{Sr} and M_S are the isotopic masses of Sr and S, respectively. The constants determined by fitting these equations to a combined data set comprising this work and that data recorded by Halfen et al.[27] are given in Tables 7 and 8. Table 7 displays the mass independent terms, U_{kl}. Table 8 displays the mass-dependent Dunham terms, Y_{kl}.

Table 7
Mass Independent Dunham Parameters for SrS[a]

Parameter	Value
U_{01}/u (MHz)	84906.76(15)[b]
U_{02}/u^2 (MHz)	-0.770453(38)
U_{03}/u^3 (MHz)	-0.00000106(10)
$U_{11}/u^{3/2}$ (MHz)	-1591.51(10)
$U_{12}/u^{5/2}$ (MHz)	-0.01686(15)
U_{21}/u^2 (MHz)	-132.19(31)
U_{22}/u^3 (MHz)	-0.00078(25)
$U_{31}/u^{5/2}$ (MHz)	119.39(26)
Δ^{Sr}_{00}	-0.78(30)
Δ^{O}_{01}	-3.773(56)

[a]These parameters have been obtained from a fit to the data in Table 5 and that data given in Ref. [27]
[b]Numbers in parentheses are one standard deviation in units of the last significant figure.

Table 8

Mass-Dependent[a] Dunham Parameters for Four Isotopomers of SrS

Parameter[c]	Y_{01} (MHz)	10^3Y_{02} (MHz)	$10^{11}Y_{03}$ (MHz)	Y_{11} (MHz)	10^6Y_{12} (MHz)	Y_{21} (MHz)	10^8Y_{22} (MHz)	Y_{31} (MHz)	r_e[b] (Å)
	B_e	-10^3De	$10^{11}H_e$	α_e	$10^6\alpha_{eD}$	Ye	108ceD	ε^e	
$^{88}Sr^{32}S$	3621.28738[d]	-1.4016775	-8.22	-14.0196441	-6.3369	-0.240489	-6.05979	0.04486	2.4397908(18)[d]
$^{87}Sr^{32}S$	3632.3639	-1.4102655	-8.30	-14.0840177	-6.3855	-0.241962	-6.11557	0.0452	2.4397908(18)
$^{86}Sr^{32}S$	3643.7305	-1.4191056	-8.38	-14.1501797	-6.4355	-0.243479	-6.17316	0.04555	2.4397909(18)
$^{88}Sr^{34}S$	3465.2774	-1.2834969	-7.21	-13.1234201	-5.6762	-0.220213	-5.30980	0.04018	2.4397861(18)

[a]The mass-dependent Dunham parameters, Y_{kl}, have been obtained from the mass-independent parameters, Ukl given in Table 7.

[b]Calculated from Y_{01} using $Y_{01} = h/8\pi^2\mu r^2_e$ where μ is the atomic reduced mass.

[c]Band constants to which Y_{kl} are approximately equal.

[d]Numbers in parentheses are one standard deviation in units of the last significant digits.

2.3.2 Internuclear Separation

Equilibrium internuclear separations, r_e, for each isotopomer, derived from Y_{01}, are given in Table 8. It is noted that the r_e values vary by amounts beyond the uncertainty that can be attributed to them. This observed mass dependence of the minimum of the potential energy surface is consistent with the measurements exceeding the limit of the Born–Oppenheimer approximation. The equation of Bunker[29]

$$U_{01} = \frac{h}{8\pi^2 (r_e^{BO})^2} \quad (8)$$

has been used to obtain r_e^{BO}, the internuclear separation at the bottom of the Born–Oppenheimer potential. The value obtained is 2.4397045(22) Å.

2.3.3 Estimates of the Vibration Frequency, Anharmonicity Constant and Dissociation Energy from Pure Rotational Data

Kratzer[30] and Pekeris[31] have produced equations that enable the vibration frequency, ω_e, and the anhamronicity constant, $\omega_e x_e$ for a diatomic molecule to be evaluated from the constants obtained in this work. The equations are

$$Y_{10} = \omega_e = \sqrt{\frac{4Y_{01}^3}{Y_{02}}} \quad (9)$$

$$Y_{20} = \omega_e x_e = Y_{01}\left(\frac{Y_{11}Y_{10}}{6Y_{01}^2} + 1\right)^2 \quad (10)$$

It is found that ω_e = 388(5) cm^{-1} and $\omega_e x_e$ = 1.14(8) cm^{-1}, in excellent agreement with the literature values of 388.2643(11) cm^{-1} and 1.28032(38) cm^{-1}, respectively[26].

Given the success of these formulae to predict ω_e and $\omega_e x_e$ it seems feasible to estimate the dissociation energy, E_{diss}, for SrS from the constants obtained above using:

$$E_{diss} = \frac{\omega_e^2}{4\omega_e x_e} \quad (11)$$

The value obtained is 395 kJ mol^{-1}. This value is in poor agreement with the literature value of 335(15) kJ mol^{-1} obtained from high temperature mass spectrometry[32]. The reason for this discrepancy lies in the underestimated $\omega_e x_e$ value obtained from equation 8. If the $\omega_e x_e$ value from Pianalto and co-workers [26] is used in Eq. (9) a value of 352 kJ mol^{-1} is obtained for the dissociation energy. This is in much better agreement with the literature value.

2.3.4 ^{87}Sr Nuclear Quadrupole Coupling Constant

The vibrational ground state nuclear quadrupole coupling constant, eQq(^{87}Sr), in ^{87}Sr^{32}S has been determined for the first time. Its value is recorded in Table 9 together with the analogous value for SrO. It was observed that eQq(^{87}S) in ^{87}Sr^{32}S is the same sign but approximately half the value found in ^{87}Sr^{16}O. The ground state configuration of Sr is [Kr] 5s^2. This configuration possesses spherical symmetry in its electron distribution and therefore has a zero eQq(^{87}Sr) value. The same story holds for the Sr^{2+} ion. A known fact is that *s*-electrons make only small contributions to eQq values[33]. One might speculate that the magnitude of the eQq(^{87}Sr) values in both molecules is caused by electron charge cloud distortion about the Sr nucleus due to the presence of the negative counter ion. The increased charge of the O ion compared to the S ion causing a larger distortion in SrO than in SrS.

Table 9
^{87}Strontium Nuclear Quadrupole Coupling Constants in SrO and SrS

MHz	$eQq(^{87}Sr)$
$^{87}Sr^{16}O$	-42.729(37)[a,b]
$^{87}Sr^{32}S$	-21.959(85)

[a]Ref. [34].

[b]Numbers in parentheses are one standard deviation in units of the last significant figure.

2.3.5 Born–Oppenheimer Breakdown Terms

Watson has derived the following expansion for the BOB terms of a diatomic molecule AB[28b, c]:

$$\Delta_{01}^{A} = \left(\Delta_{01}^{A}\right)^{ad} + \frac{(\mu g_J)_B}{m_P} + \frac{\mu \Delta Y_{01}^{(D)}}{m_e B_e} \quad (12)$$

Here, $\left(\Delta_{01}^{A}\right)^{ad}$ represents the adiabatic contribution to Δ_{01}^{A}, m_p is the mass of the proton, $\Delta Y_{01}^{(D)}$ is the Dunham correction[28a], and $\left(\mu g_J\right)_B$ is the isotopically independent value of μg_J referred to nucleus B as the origin:

$$(\mu g_J)_B = \mu g_J + 2c_A m_P M_A/(M_A + M_B), \quad (13)$$

where c_A is the formal charge on atom A derived from the dipole moment, D, and the charge on the electron, e, according to $|c_A| = \left|\frac{D}{er_e}\right|$. Naturally, there is a corresponding expression for Δ_{01}^{B}. Watson has demonstrated that although Δ_{01}^{A} should not be equal to Δ_{01}^{B}they should be reasonably close in magnitude. Watson has further demonstrated that the anticipated magnitudes of the BOB terms should be on the order of unity. Indeed, as a demonstration of the theory BOB terms were determined for CO. The updated values are Δ_{01}^{C} = -2.0545(12) and Δ_{01}^{O} = -2.0982(13)[35]. There is a small but

growing literature surrounding BOB terms and an extended listing of determined values is given in Table 10. On the basis of BOB terms there appear several classes of molecule. Firstly, like CO, there exist a normal class for which, say, 0 > $\Delta_{01}^{A} \approx \Delta_{01}^{B}$ > -5. There is then a second class of molecules for which an initial analysis yields $\Delta_{01}^{A} \gg \Delta_{01}^{B}$. Members of this class appear to exclusively include molecules in which one atom is heavy, i.e. Z > ≈50. Examples include PtSi[36], PbS and TlF[37]. This situation strongly indicates that field shift effects are detectable in the spectra[37a]. Fitting field shift parameters, V_{01}^{i}, returns the BOB terms to more normal magnitudes. A third class of molecule produces $\Delta_{01}^{A} \approx \Delta_{01}^{B} \ll$ -10, see for example TeSe[38] and SbCl[39]. BOB terms of very large magnitude accompany the analysis of heavy molecules that have $^{3}\Sigma^{+}$ ground states in Hund's coupling case (a) but are well described by Hund's coupling case (c). The observed $\Omega = 0^{+}$ ground state appears, in all respects (apart from the magnitudes of the BOB terms), to mimic a $^{1}\Sigma^{+}$ electronic symmetry. A few molecules have been studied that appear to fall into both the second and third categories described above, i.e. they possess $X0^{+}$ electronic ground states and initial analyses have indicated the presence of field shift effects. Examples of this situation include PtO[40] and PtS[41].

SrS appears "normal", although Δ_{01}^{Sr} is somewhat less than Δ_{01}^{S}. In the analyses of SnS and PbS, Knöckel and Tiemann show that whilst field shift effects were important in analyzing the PbS rotational spectra they were of negligible importance in the analysis of SnS. With Sr being lighter than Sn and field shift parameters being proportional to Z field shift effects are unlikely to be a major factor behind the difference in magnitude for the SrS BOB terms. Just as the case for ZrO, ZrS[42] and

HfS[43] non-adiabatic effects are most likely the cause for the magnitudes of the SrS BOB terms. Unfortunately, in the absence of a rotational g_{J-} factor further discussion is prohibited.

Table 10
Watson-Type Δ_{01}Terms, Field Shift eTrms V^{A}_{01} (where known), and Mass Reduced Dunham-Type Coefficient U_{01} for Several Diatomic Molecules

AB	Δ^{A}_{01}	Δ^{B}_{01}	$V^{A}_{01}/10^{-7}$ (fm^{-2})	U_{01}/u (MHz)	Ref.
HCl	-0.26(20)	0.1262(8)		311077.90(96)	[44]
CO	-2.0545(12)	-2.0982(13)		397029.003(24)	[35]
CS	-2.596(49)	-2.223(98)		214536.32(64)	[37b]
NaCl	—	-0.84558(926)		90678.9425(143)	[45]
AlCl	—	-1.443(29)		111378.117(49)	[46]
SiS	-1.392(59)	-1.870(65)		135779.38(27)	[37b]
ClO	-1.419(24)	-2.240(13)		205150.59(13)	[47]
KCl	0.3628(626)	-1.28012(448)		71070.74627(848)	[45]
GaH	-2.62(35)	-4.2181(13)		183363.95(42)	[48]
GaF	-0.60(30)	—		160526.16(45)[g]	[37b]
GaI	-0.706(96)	—		76241.02(24)[g]	[37b]
GeS	-1.463(70)	-1.871(45)		124836.77(12)[g]	[37b]
GeSe	-1.505(87)	-1.86(14)		110913.1(82)	[49]
	-1.612(46)	-2.014(69)		110913.23(10)	[37b]
BrO	-1.124(48)	-1.963(4)		170697.68(6)	[50]
SrS	-0.78(30)	-3.773(56)		84906.76(15)	[51]
ZrO	-4.872(39)	-6.1888(25)		172480.086(98)	[42]
ZrS	-5.325(82)	-6.523(39)		108670.07(19)	[42]
InI	-2.68(27)	—		66651.46(48)	[37b]
			10		[52]
SnS	-1.76(19)	-1.821(65)		103569.62(21)	[37b]
SnSe	-1.555(84)	-2.124(50)		93445.166(88)	[37b]
			2.0(6)		[52]
			13.1[r]		[53]
SnTe	-1.749(97)	-2.120(76)		79405.790(82)	[37b]
			3.1(7)		[52]
			12.5[f]		[53]
SbF	-36.17(81)	-36.2(10)[c]		137438.3(40)	[39]
SbCl	-26.1(23)	-26.19(30)		92654.5(11)	[39]
SbN	-2.52(47)	-2.609(17)		149995.47(33)	[54]
SbP	-3.1(9)	-3(1)[c]		103909(2)	[54]

TeSe	-20.9787(71)	-20.9541(32)		90812.6656(10)	[38]
IO	—	-2.213(9)		143542.72(20)	[55]
LuCl	-2.98c	-2.98(12)	2.4[r]		[56]
HfO	-3.40(57)	-5.656(23)		170239.68(18)[g]	[57]
HfS	-4.18(53)	-5.820(49)		108708.38(27)	[39]
PtO	-43.73(70)a	-70.477(16)		169834.60(35)[b]	[40]
PtO[h]	-70.5(10)c	-70.46(2)	-145(5)	$\tilde{U}_{01}$=135004.17(10)[d]	
				U_{01}=134991.08(45)	
			-133[f]		
PtSi	10.75(68)	-2.99(4)		118923.32(33)[b]	[36]
PtSi[h]	-3(1)c	-2.99(4)	-72(12)	$\tilde{U}_{01}$=118927.94(54)[d]	
				U_{01}=118952.7(47)[c]	
			-110[f]		
PtS	-42.60(74)	-62.466(49)		121604.07(30)[b]	[41]
PtSi[h]	-62.5(10)c	-62.46(5)	-104(9)	$\tilde{U}_{01}$=121610.91(50)[d]	
		121647.1(20)[e]		U_{01}=121647.1(20)[c]	
			-84[f]		
TlF	-18.76(110)	—		116321.7(11)[g]	[37b]
TlF[h]	-0.341i	—	40.9(19)	40.9(19)	[52]
			77.0[f]		[53]
TlCl	18.96(200)	-1.243(49)		81857.0(1)[g]	[37b]
TlCl[h]	-0.500i	-1.257(73)	40.9(55)	40.9(55)	[52]
			88.0[f]		[53]
TlBr	-15.61(46)	-1.138(64)		73729.425(84)[g]	[37b]
TlBr[h]	-0.423i	-1.138(64)	33.7(10)	33.7(10)	[52]
			67.7[f]		[53]
TlI	-14.68(47)	—		63839.29(45)[g]	[37b]
TlI[h]	-0.263i	—	32.0(10)	32.0(10)	[52]
			60.9[f]		[53]
PbS	-12.94(141)	-1.997(71)		96642.20(50)[g]	[37b]
PbS[h]	-1.333i	-1.988(70)	26.38(51)	26.38(51)	[37a]
			34.5[f]		[53]
PbSe[h]	-1.520i	-2.094(72)	22.1(19)	22.1(19)	[52]
			34.7[f]		[53]
PbTe	-11.98(81)	-1.794(110)		75052.88(16)[g]	[37b]
PbTe[h]	-1.405i	-1.84(11)	21.2(16)	21.2(16)	[52]
			32.8[f]		[53]

BiN	—	-2.788(19)		135003.18(10)[b]	[58]
	-2.8(10)c	-2.788(19)	32[r]	$\bar{U}_{01}$=135004.17(10)[d]	
				U_{01}=134991.08(45)	

2.4 Conclusions

The pure rotational spectra of four isotopomers of SrS have successfully recorded in the 6–26 GHz region. The SrS internuclear separation has been determined with a significant improvement in precision. The eQq(^{87}Sr) value in SrS has been measured and compared to the value in SrO. It is likely that electron charge cloud distortion from the S ion is the likely cause of the parameters magnitude. Lastly, the BOB terms for both atoms in SrS have been determined. These values have been added to an extensive table of BOB values.

CHAPTER 3[3]

THE PURE ROTATIONAL SPECTRUM OF THE ACTINIDE-CONTAINING COMPOUND THORIUM MONOXIDE

The J = 1–0 pure rotational transition, together with hyperfine structure where appropriate, has been recorded for all three naturally occurring isotopomers of the actinide-containing compound thorium monoxide ($^{232}Th^{16}O$, $^{232}Th^{17}O$ and $^{232}Th^{18}O$).

The first pure rotational spectroscopic investigation of any actinide-containing compound was completed in this experiment. Thorium monoxide has been prepared by laser ablation of Th metal in the presence of oxygen and has subsequently been observed using a Fourier transform microwave spectrometer. The J = 1–0 transition has been measured in a variety of vibrational states and for all three naturally occurring isotopomers. Hyperfine structure has been recorded for the $^{232}Th^{17}O$ isotopomer giving unique insight into the ThO chemical bond and the electronic structure of the molecule.

Detailed experimental studies of actinide chemistry are required due to the interests and concerns that surround these elements, particularly thorium, as sources of nuclear fuel. Two reasons underlie the scarcity of fundamental experimental data for actinide compounds. The first reason is the complexity of the problem. Experimental observations are difficult to interpret; electron correlation, relativistic effects and numerous, easily accessible electronic states result in actinide compounds being a thorny problem for correct theoretical treatment. The second reason is the inherent

[3] This entire chapter is reproduced from Dewberry, C. T.; Etchison, K. C.; Cooke, S. A., The pure rotational spectrum of the actinide-containing compound thorium monoxide. Physical Chemistry Chemical Physics 2007, 9 (35), 4833-4940, with permission of the PCCP Owner Societies. http://www.rsc.org/

danger, and therefore expense, of handling actinide species, which are both radioactive and highly toxic.

A very small number of experimental groups have, in part, overcome these difficulties[59]. Edvinsson and Lagerqvist have studied the electronic spectra of ThO; numerous band systems were observed and many studied with rotational resolution[59a]. Kushto and Andrews used matrix isolation spectroscopy to study the rich chemistry resulting from ablating thorium in the presence of NO_2[59b]. However, ThO, and actinide compounds in general, attract greatest attention from the computational chemistry community[60]. Clearly, there is a desire, from a safety standpoint, to perform actinide chemistry on a computer. ThO is a prototype actinide system for computational chemistry and serves as a useful molecule for testing new methodologies.

Despite the molecule's importance, a great deal remains unknown about ThO. The provision of spectroscopic hyperfine constants will be very useful in addressing these unknowns by providing experimental insight into the molecule's electronic structure. In this work, pure rotational spectra for ThO, X $^1\Sigma^+$, have been recorded using a newly constructed Balle–Flygare Fourier transform microwave spectrometer[1], the details of which will be presented elsewhere. Samples entrained in pulsed jets of a noble gas mix were injected into a Fabry-Perót cavity cell. As a consequence of the pulsed gas jet and microwave propagation axis being parallel all transitions were observed as doublets due to the Doppler effect. Line widths for ThO were 7 kHz. Time critical aspects of the experiment were referenced to a stable cesium frequency standard and all measurements are accurate to ±1 kHz or better.

A piece of thorium foil, which was wrapped around a cylindrical support and held at the nozzle's exit orifice, was ablated with a pulse of radiation (λ = 1064 nm) from a Nd:YAG laser in the presence of 0.1% O_2 gas in a 30 : 70 He : Ne gas mix.

Only the J = 1–0 transition of ThO fell within the range of our spectrometer. However, this transition is sufficient to allow examination of the molecules internuclear potential with unprecedented accuracy. The data obtained are given in Table 11.

Table 11
Measured Transition Frequencies in MHz for Three Isotopomers of ThO

Isotope	v	F'-F"	Frequency (MHz)			Obs - Calc (kHz)
$^{232}Th^{16}O$	0				19904.4756	-5.6
	1				19826.2165	-1.2
	2				19747.7977	1.7
	3				19669.2191	3.1
	4				19590.4795	1.8
	5				19511.5778	-3.3
	6				19432.5218	-4.4
	7				19353.3168	3.8
$^{232}Th^{17}O$		3/2 - 5/2	18805.3640			
	0	7/2 - 5/2	18805.5492	18805.7266[a]		4.9
		5/2 - 5/2	18806.1830			
		3/2 - 5/2	18733.5014			
	1	7/2 - 5/2	18733.6890	18733.8641[a]		4.4
		5/2 - 5/2	18734.3186			
$^{232}Th^{18}O$	0				17833.2850	0.4
	1				17766.9301	-3.6
	2				17700.4537	-1.7

[a] Hypothetical unsplit frequencies

The use of isotopically enriched $^{17}O_2$ (10% abundance, Icon Isotopes Ltd) permitted the study of both the $^{232}Th^{17}O$ and $^{232}Th^{18}O$ isotopomers. A sample piece of data is given in Figure 9.

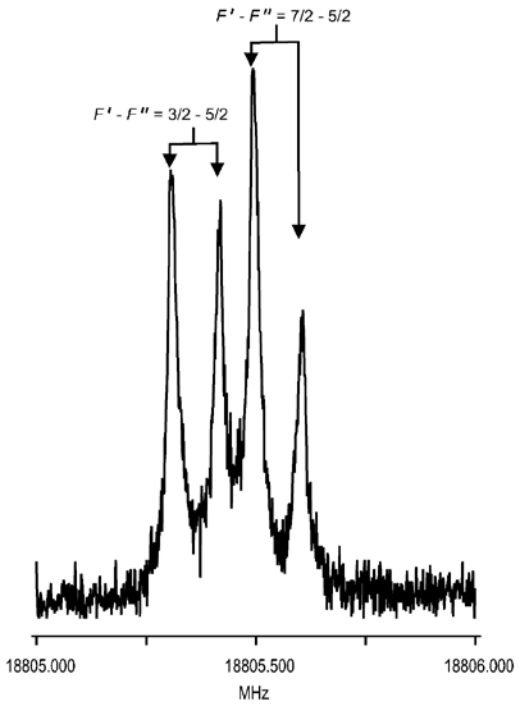

Figure 9. Two hyperfine components from the J = 1–0, v = 0 transition for $^{232}Th^{17}O$.

The Fourier transformation shown is the result of 6000 averaging cycles. The components appear as doublets due to the Doppler effect.

Hyperfine structure arising from the coupling of the nuclear spin of ^{17}O (I=5/2) with the end-over-end rotation of the ThO molecule was easily observed.

Molecular constants were derived from the observed transitions in the following way. Initially the $^{232}Th^{17}O$ data were treated. The rotational constant, B, nuclear quadrupole coupling constant, eQq(^{17}O), and nuclear spin–rotation constant, CI(^{17}O), were obtained from fitting an effective Hamiltonian to the line frequencies shown in Table 11. Constants for both the ν = 0 and 1 states were obtained separately. The rotational constants obtained were then doubled to obtain the hypothetical, unsplit J = 1–0 frequencies for the ν = 0 and 1 states. These frequencies, together with the transition frequencies for $^{232}Th^{16}O$ and $^{232}Th^{18}O$ were then used in a Dunham type, multi-isotopomer, multi-vibrational state fitting routine[28a]. To the accuracy of the present work, with the exception of Y_{01}, each $Y_{kl} = U_{kl}\mu^{-(k+2l)/2}$, with U_{kl} being a mass-independent Dunham parameter. The parameter Y_{01} is given by:

$$Y_{01} = \frac{U_{01}}{\mu}\left[1 + m_e\left(\frac{\Delta_{01}^{Th}}{M_{Th}} + \frac{\Delta_{01}^{O}}{M_O}\right)\right] \quad (14)$$

Here, m_e, is the rest mass of the electron and M_{Th} and M_O are the masses of the Th and O atoms, respectively. The Δ_{01}^{i}terms are Watson's isotopically independent Born–Oppenheimer breakdown terms for atoms i[28b]. Note that effects due to the nuclear volume of thorium, i.e. field shift effects,[61] are not determinable from the data set and are therefore not considered. Naturally occurring thorium is mono-isotopic and so $\square_{01}^{T}$ is also not determinable from the data set obtained. The constants determined during the fitting process are given in Table 12.

Table 12
Determined Spectroscopic Parameters for ThO

Parameter	Value[a]
Y_{01}/MHz	9971.7767(35)
U_{01}/u MHz	149242.742(52)
Y_{11}/MHz	-39.05256(26)
Y_{21}/MHz	-0.039573(33)
Δ_{01}^{O}	-5.970(11)
eQq(^{17}O) v = 0/MHz	2.827(9)
eQq(^{17}O) v = 1/MHz	2.815(9)
CI(^{17}O) v = 0/MHz	-0.0108(5)
CI(^{17}O) v = 1/MHz	-0.0110(5)
r_e^{BO}, /Å	1.84018613(24)[b]

[a]Numbers in parenthesis indicate one standard deviation in units of the least significant figure.
[b]Allowing $\Delta_{01}^{Th} = \Delta_{01}^{O} \pm 1$ causing the uncertainty of this figure to increase by one order of magnitude, see text for discussion.

The internuclear separation at the bottom of the isotopically independent Born–Oppenheimer potential, r_e^{BO}, has been determined for ThO from the mass independent U_{01} parameter[29]. The value obtained is given in Table 12. Note that by allowing the reasonable assumption that $\Delta_{01}^{Th} = \Delta_{01}^{O} \pm 1$ the U_{01} parameter is adjusted and a variation in r_e^{BO} of ±13 X 10^{-6} Å results. Also note, once again, that field shift effects have been

neglected. In order to err on the side of caution, the uncertainty in r_e^{BO} should be considered an order of magnitude larger than that given in Table 12 such that r_e^{BO}=1.840186(2) Å.

The magnitudes of the Born–Oppenheimer breakdown parameters are intimately linked to the electronic structure of the molecule. They contain both adiabatic and non adiabatic contributions[28b]. The Δ_{01}^{O}term in ThO, -5.970(11), is intermediate between the values obtained for oxygen in both ZrO,[42] Δ_{01}^{O} = -6.1888(25), and HfO,[57] Δ_{01}^{O} = -5.656(23). The similar magnitudes of the Δ_{01}^{O} terms for ZrO, HfO and ThO provide direct and unique evidence indicating the comparable, and clearly complex, molecular electronic structures for all three molecules.

For $^{232}Th^{17}O$ we have determined the nuclear quadrupole coupling constant, eQq(^{17}O), and the nuclear spin–rotation constant, C_I(^{17}O). Equilibrium values for these constants may be obtained by fitting the vibrational dependent constants to the expression $X_v = X_e + X_I(v + 1/2)$. The values obtained from solving the two simultaneous equations are eQq_e(^{17}O) = 2.833(10) MHz and C_{Ie}(^{17}O) = -0.0107(6) MHz.

The value of eQq(^{17}O) may be directly related to the value of the quadrupole moment of ^{17}O, and the electric field gradient at that nucleus. For the O^{2-} ion the eQq(^{17}O) value is zero due to the spherical symmetry of the electron distribution about the nucleus. For the O atom, ($^3P_2$), eQq(^{17}O) = 10.438(30) MHz.14 The eQq(^{17}O) value of 2.833(10) MHz for $Th^{17}O$ is consistent with an appreciably ionic structure. The charge on Th in ThO has been calculated to be between +0.5 e and +0.7 e.[3,4]. The eQq(^{17}O) value for $Th^{17}O$ suggests that the charge on Th is at the upper end, and possibly

beyond, the calculated range. Similarities have been drawn over the electronic structure, and therefore chemistry, of thorium, [Rn] $6d^2 7s^2$, and the Group 4 transition metals, (Ti, Zr, Hf), all of which are $nd^2 n + 1s^2$; and also with the $ns^2 np^2$ carbon family[62]. As discussed above the determined Δ_{01}^{0} term supports the first comparison. The second comparison may be examined using the eQq(^{17}O) constant. For C^{17}O, eQq(^{17}O) has been determined to be 4.3205(7) MHz.16 From the ^{17}O quadrupole moment[63] the field gradient at the ^{17}O nucleus in C^{17}O was calculated to be -6.985 X 10^{21} V m^{-2}. The negative of the ratio of this molecular value with the atomic value[63] gives the deficit or excess of *p*-electrons along the internuclear axis. For C^{17}O a deficit of 0.4 *p*-electrons along the internuclear axis was calculated. Using the same treatment, a deficit of 0.27 *p*-electrons along the internuclear axis in ThO was also found. The bond in ThO is formed between an interaction between the Th $d\sigma$ and $d\pi$ electrons and the O $p\sigma$ and $p\pi$ electrons[60a]. The arguments above show that electron donation from Th *d*-orbitals to O *p*-orbitals is more complete than the donation from C *p*-orbitals to O *p*-orbitals in CO. Determination of the eQq(^{17}O) values in ZrO, HfO, SnO and PbO will shed further light on the bonding in ThO. The results presented here indicate a new source of experimental data for actinide-containing species.

REFERENCES

1. Balle, T. J.; Flygare, W. H., Fabry-Perot cavity pulsed Fourier transform microwave spectrometer with a pulsed nozzle particle source. *Review of Scientific Instruments* **1981,** *52* (1), 33-45.

2. Grabow, J.-U.; Stahl, W.; Dreizler, H., A multioctave coaxially oriented beam-resonator arrangement Fourier-transform microwave spectrometer. *Review of Scientific Instruments* **1996,** *67* (12), 4072-4084.

3. Grabow, J.-U.; Palmer, E. S.; McCarthy, M. C.; Thaddeus, P., Supersonic-jet cryogenic-resonator coaxially oriented beam-resonator arrangement Fourier transform microwave spectrometer. *Review of Scientific Instruments* **2005,** *76* (9), 093106-093107.

4. Kolbe, W. F.; Leskovar, B., 140-GHZ pulsed Fourier transform microwave spectrometer. *Review of Scientific Instruments* **1985,** *56* (1), 97-103.

5. Braakman, R.; Kelley, M. J.; Cossel, K.; Blake, G. A. In *EXTENDING THE PRINCIPLES OF THE FLYGARE: TOWARDS A FOURIER TRANSFORM THz SPECTROMETER.*, 61st Ohio State University International Symposium on Molecular Spectroscopy., Columbus, Ohio, Columbus, Ohio, 2006.

6. Arunan, E.; Emilsson, T.; Gutowsky, H. S., Rotational spectra and structures of Rg-C_6H_6-H_20 trimers and the Ne-CsHs dimer (Rg=Ne, Ar, or Kr). *Journal of Chemical Physics* **1994,** *101* (2), 861-868.

7. Storm, V.; Breizler, H.; Consalvo, D.; Grabow, J.-U.; Merke, I., A newly designed molecular beam Fourier transform microwave spectrometer in the range 1–4 GHz. *Review of Scientific Instruments* **1996,** *67* (8), 2714-2719.

8. Suenram, R. D.; Lovas, F. J.; Fraser, G. T.; Matsumura, K., Pulsed-nozzle Fourier-transform microwave spectroscopy of laser-vaporized metal oxides: Rotational spectra and electric dipole moments of YO, LaO, ZrO, and HfO. *Journal of Chemical Physics* **1990,** *92* (8), 4724-4734.

9. Harmony, M. D.; Beran, K. A.; Angst, D. M.; Ratzlaff, K. L., A compact hot-nozzle Fourier-transform microwave spectrometer. *Review of Scientific Instruments* **1995,** *66* (11), 5196-5203.

10. Walker, K. A.; Gerry, M. C. L., Microwave Fourier Transform Spectroscopy of Magnesium Sulfide Produced by Laser Ablation. *Journal of Molecular Spectroscopy* **1997,** *182* (1), 178-183.

11. Lesarri, A.; Mata, S.; López, J. C.; Aionso, J. L., A laser-ablation molecular-beam Fourier-transform microwave spectrometer: The rotational spectrum of organic solids. *Review of Scientific Instruments* **2003,** *74* (11), 4799 - 4805.

12. Drouin, B. J.; Cassak, P. A.; Briggs, P. M.; Kukolich, S. G., Determination of structural parameters for the half-sandwich compounds cyclopentadienyl thallium and cyclopentadienyl indium and indium quadrupole coupling for cyclopentadienyl indium using microwave spectroscopy. *Journal of Chemical Physics* **1997,** *107* (10), 3766 - 3774.

13. Wötzel, U.; Harder, H.; Mäder, H., Radiofrequency spectra of ethyl fluoride recorded with two-dimensional Fourier transform spectroscopy using a coaxial sample cell. *Journal of Molecular Spectroscopy* **2001,** *599* (1-3), 317 - 321.

14. Auchterlonie, L. J.; Ahmed, I. Y., Microwave wideband open resonator of large aperture. *Journal of Physics E: Scientific Instruments* **1977,** *10* (7), 691-695.

15. Clarke, R. N.; Rosenberg, C. B., Fabry-Perot and open resonators at microwave and millimetre wave frequencies, 2-300GHz. *Journal of Physics E: Scientific Instruments* **1982,** *15* (1), 9-25.

16. Stein, S. R.; Turneaure, J. P., SuperconductingCavity Stabilized Oscillators with Improved Frequency Stability. *Proceedings of the IEEE* **1975,** *63* (8), 1249-1250.

17. Siegman, A. E., Unstable Optical Resonators for Laser Applications. *Proceedings of the IEEE* **1965,** *53* (3), 277-287.

18. Siegman, A. E., Laser beams and resonators: Beyond the 1960's. *IEEE Journal of Selected Topics in Quantum Electronics* **2000,** *6* (6), 1389-1399.

19. Chantry, G. W., The use of Fabry-Perot interferometers, etalons and resonators at infrared and longer wavelengths-an overview. *journal of Physics E: Scientific Instruments* **1982,** *15* (1), 3-9.

20. Kogelnik, H.; Li, T., Laser Beams and Resonators. *Applied Optics* **1966,** *5* (10), 1550-1567.

21. Grabow, J.-U. *FTMW++*.

22. Peebles, S. A.; Peebles, R. A., Determination of the heavy atom structure of bromobenzene by rotational spectroscopy. *Journal of Molecular Structure* **2003,** *657* (1-3), 107-116.

23. Mirri, A. M.; Caminati, W., Quadrupole hyperfine structure in the rotational spectrum of iodobenzene. *Chemical Physics Letters* **1971,** *8* (5), 409-124.

24. Huang, H.; Sullivan, V., The solution dipole moments and the atomic polarizations of chloro-, bromo-, and iodo-benzenes. *Australian Journal of Chemistry* **1968,** *21* (7), 1721-1725.

25. Pickett, H. M., The Fitting and Prediction of Vibration-Rotation Spectra with Spin Interactions. *Journal of Molecular Spectroscopy* **1991,** *148* (2), 371-377.

26. Pianalto, F. S.; Brazier, C. R.; O'Brien, L. C.; Bernath, P. F., Rotational analysis of the $A^1\Sigma^+$-$X^1\Sigma^+$ transition of SrS *Journal of Molecular Spectroscopy* **1988,** *132* (1), 80-88.

27. Halfen, D. T.; Apponi, A. J.; Thompsen, J. M.; Ziurys, L. M., The pure rotational spectra of SrSH (X^2A') and SrS ($X^1\Sigma^+$): Further studies in alkaline-earth bonding *Journal of Chemical Physics* **2001,** *115* (24), 11131-11138.

28. (a) Dunham, J. L., The Energy Levels of a Rotating Vibrator. *Physical Review* **1932,** *41*, 721-731; (b) Watson, J. K. G., The Isotope Dependence of Diatomic Dunham Coefficients. *Journal of Molecular Spectroscopy* **1980,** *80* (2), 411-421; (c) Watson, J. K. G., The Isotope Dependence of the Equilibrium Rotational Constants in $^1\Sigma$ States of Diatomic Molecules. *Journal of Molecular Spectroscopy* **1973,** *45*, 99-113.

29. Bunker, P. R., The Nuclear Mass Dependence of the Dunham Coefficients and the Breakdown of the Born-Oppenheimer Approximations. *Journal of Molecular Spectroscopy* **1977,** *68*, 367-371.

30. Kratzer, A., Die ultraroten Rotationsspektren der Halogenwasserstoffe. *Zeitschrift für Physik A Hadrons and Nuclei* **1920,** *3* (5), 289-307.

31. Pekeris, C. L., The Rotation-Vibration Coupling in Diatomic Molecules. *Physical Review* **1934,** *45*, 98-103.

32. Cater, E. D.; Johnson, E. W., Sublimation of Strontium Sulfide and the Dissociation Energy of SrS. *The Journal of Chemical Physics* **1967,** *47*, 5353-5357.

33. Gordy, W.; Cook, R. L., *Microwave Molecular Spectra: Techniques in Chemistry, Vol. XVIII*. Wiley: New York, 1984.

34. Blom, C. E.; Hedderich, H. G.; Lovas, F. J.; Suenram, R. D.; Maki, A. G., Infrared and microwave spectra of SrO and BaO. *Journal of Molecular Spectroscopy* **1992,** *152* (1), 109-118.

35. Authier, N.; Bagland, N.; Lefloch, A., The 1992 Evaluation of Mass-Independent Dunham Parameters for the Ground State of CO. *Journal of Molecular Spectroscopy* **1993,** *160* (2), 590-592.

36. Cooke, S. A.; Gerry, M. C. L.; Brugh, D. J.; Suenram, R. D., The rotational spectrum, nuclear field shift effects, 195Pt nuclear spin–rotation constant, and electric dipole moment of PtSi. *Journal of Molecular Spectroscopy* **2004,** *223* (2), 185-194.

37. (a) Knöckel, H.; Tiemann, E., Isotopic field shift in the transition A 0++—X1∑+ of PbS. *Chemical Physics* **1982,** *68* (1-2), 13-19; (b) Tiemann, E.; Stieda, W. U.; Torring, T.; Hoeft, J., *Z. Naturforsch.* **1975,** *30a*.

38. Banser, D.; Grabow, J.-U.; Cocinero, E. J.; Lesarri, A.; Alonso, J. L., The pure rotational spectrum of TeSe: Rotational parameters, Born–Oppenheimer breakdown corrections, and hyperfine constants. *Journal of Molecular Structure* **2006,** *795* (1-3), 163-172.

39. Cooke, S. A.; Gerry, M. C. L., Born-Oppenheimer breakdown effects and hyperfine structure in the rotational spectra of SbF and SbCl. *Journal of Molecular Spectroscopy* **2005,** *234*, 195-203.

40. Cooke, S. A.; Gerry, M. C. L., The influence of nuclear volume and electronic structure on the rotational energy of platinum monoxide, PtO. *Physical Chemistry Chemical Physics* **2005,** *7* (12).

41. Cooke, S. A.; Gerry, M. C. L., Internuclear distance and effects of Born–Oppenheimer breakdown for PtS, determined from its pure rotational spectrum. *Journal of Chemical Physics* **2004,** *121* (8), 3486-3495.

42. Beaton, S. A.; Gerry, M. C. L., Rotational spectra and hyperfine constants of ZrO and ZrS. *Journal of Chemical Physics* **1999,** *110* (22), 10715-10725.

43. Cooke, S. A.; Gerry, M. C. L., The Pure Rotational Spectrum, Geometry, and Hyperfine Constants of Hafnium Monosulfide, HfS. *Journal of Molecular Spectroscopy* **2002,** *216* (1), 122-130.

44. Guelachvili, G.; Niay, P.; Bernage, P., Infrared bands of HCl and DCl by Fourier transform spectroscopy : Dunham coefficients for HCl, DCl, and TCl. *Journal of Molecular Spectroscopy* **1981,** *85* (2), 271-281.

45. Caris, M.; Lewen, F.; Müller, H. S. P.; Winnewisser, G., Pure rotational spectroscopy of potassium chloride, KCl, up to 930 GHz and isotopically invariant analysis of KCl and NaCl. *Journal of Molecular Structure* **2004,** *695-696*, 243-251.

46. Hedderich, H. G.; Dulick, M.; Bernath, P. F., High resolution emission spectroscopy of AlCl at 20 μ. *Journal of Chemical Physics* **1993,** *99* (11), 8363-8371.

47. Drouin, B. J.; Miller, C. E.; Cohen, E. A.; Wagner, G.; Birk, M., Further Investigations of the ClO Rotational Spectrum. *Journal of Molecular Spectroscopy* **2001,** *207* (1), 4-9.

48. Campbell, J. M.; Dulick, M.; Klapstein, D.; White, J. B.; Bernath, P. F., High resolution infrared emission spectra of GaH and GaD. *Journal of Chemical Physics* **1993,** *99* (11), 8379-8385.

49. Konno, T.; Uehara, H., Infrared diode laser spectroscopy of a high-temperature molecule: GeSe. *Chemical Physics Letters* **1995,** *247* (5-6), 529 - 533.

50. Drouin, B. J.; Miller, C. E.; Müller, H. S. P.; Cohen, E. A., The Rotational Spectra, Isotopically Independent Parameters, and Interatomic Potentials for the X12Π3/2 and X22Π1/2 States of BrO. *Journal of Molecular Spectroscopy* **2001,** *205* (1), 128-138.

51. Etchison, K. C.; Dewberry, C. T.; Cooke, S. A., Born-Oppenheimer breakdown effects and hyperfine structure in the rotational spectrum of strontium monosulfide, SrS. *Chemical Physics* **2007,** *342* (1-3), 71-77.

52. Knockel, H.; Krockertskothen, T.; Tiemann, E., Molecular-beam-laser studies of the states X1Σ+ and A0+ of PbS. *Chemical Physics* **1985,** *93* (2), 349-358.

53. Cooke, S. A.; Gerry, M. C. L.; Chong, D. P., The calculation of field shift effects in the rotational spectra of heavy metal-containing diatomic molecules using density functional theory: comparison with experiment for the Tl-halides and Pb-chalcogenides. *Chemical Physics* **2004,** *298* (1-3), 205-212.

54. Cooke, S. A.; Gerry, M. C. L., The pure rotational spectra and hyperfine constants of SbN and SbP. *Physical Chemistry Chemical Physics* **2004,** *6* (19), 4579-4586.

55. Miller, C. E.; Cohen, E. A., Rotational spectroscopy of IO $X^2\Pi_i$. *Journal of Chemical Physics* **2001,** *115* (14), 6459-6471.

56. Cooke, S. A.; Krumrey, C.; Gerry, M. C. L., Pure rotational spectra of LuF and LuCl. *physical Chemistry Chemical Physics* **2005,** *7* (13), 2570-2579.

57. Lesarri, A.; Suenram, R. D.; Brugh, D., Rotational spectrum of jet-cooled HfO2 and HfO. *Journal of Chemical Physics* **2002,** *117* (21), 9651-9663.

58. Cooke, S. A.; Michaud, J. M.; Gerry, M. C. L., Microwave spectra, nuclear field shift effects, geometries and hyperfine constants of bismuth mononitride, BiN, and bismuth monophosphide, BiP. *Journal of Molecular Structure* **2004,** *695-696*, 13-22.

59. (a) Edvinsson, G.; Lagerqvist, A., Two New Band systems in ThO. *Physica Scripta* **1990,** *41* (3), 316-320; (b) Kushto, G. P.; Andrews, L., Infrared Spectroscopic and Density Functional Theoretical Investigation of the Reaction Products of Laser-Ablated Zr, Hf, and Th Atoms with Nitric Oxide *Journal of Physical Chemistry A* **1999,** *103* (25), 4836-4844.

60. (a) Marian, C. M.; Wahlgren, U.; Gropen, O.; Pyykkö, P., Bonding and electronic structure in diatomic ThO: Quasirelativistic effective core potential calculations. *Journal of Molecular Structure: THEOCHEM* **1988,** *169*, 339-354; (b) Watanabe, Y.; Matsuoka, O., All-electron Dirac-Fock-Roothaan calculations for the ThO molecule. *Journal of Chemical Physics* **1997,** *107* (9), 3738-3739; (c) Watanabe, Y.; Matsuoka, O., Four-component relativistic configuration-interaction calculation using the reduced frozen-core approximation. *Journal of Chemical Physics* **2002,** *116* (22), 9585-9591; (d) Paulovic, J.; Nakajima, T.; Hirao, K.; Seijo, L., Third-order Douglas–Kroll ab initio model potential for actinide elements. *Journal of Chemical Physics* **2002,** *117* (8), 3597-3605.

61. Tiemann, E.; Arnst, H.; Stieda, W. U.; Törring, T.; Hoeft, J., Observed adiabatic corrections to the born-oppenheimer approximation for diatomic molecules with ten valence electrons. *Chemical Physics* **1982,** *67* (2), 133-138.

62. Cotton, F. A.; Murillo, C. A.; Bochmann, M., *Advanced Inorganic Chemistry*. 6th Edition ed.; Wiley: New York, NY, 1999.

63. Sundholm, D.; Olsen, J., Finite element multiconfiguration Hartree-Fock calculations on carbon, oxygen, and neon: the nuclear quadrupole moments of carbon-11, oxygen-17, and neon-21. *Journal of Physical Chemistry* **1992,** *96* (2), 627-630.